ORIGINAL ARTICLE

Impact of laser process parameters in direct energy deposition on microstructure, layer characteristics, and microhardness of TC21 alloy

Ramadan Nagy Elshaer[1] · Ahmed Magdi Elshazli[2] · Abdel Hamid Ahmed Hussein[3] · Samar Reda Al-Sayed[2]

Abstract
In the present study, layers consisting of 40% Stellite-6 and 60% WC were deposited on Ti-6Al-3Mo-2Sn-2Zr-2Nb-1.5Cr-0.1Si (TC21) alloy by means of direct energy deposition (DED) technology aiming to improve the microstructure and microhardness. Five powder feeding rates ranging from 20 to 100 g min^{-1} were applied using CW fiber-coupled diode laser with 4 kW output power. The deposited layers were analyzed via scanning electron microscopy (SEM), energy-dispersive X-ray analysis (EDX), and X-ray diffractometry (XRD). The results show that WC particles are dispersed in a heterogeneous manner in the deposition zone, especially at the rates 20, 40, and 60 g min^{-1}. In addition, microcracks appeared in the interface zone particularly at 100 g min^{-1} due to the higher induced residual stresses caused by the difference in the coefficient of thermal expansion between Stellite-6, WC particles, and TC21 substrate alloy. Several complex carbides and intermetallic compounds such as W_2C, TiC, Cr_7C_3, Co_3W_3C, and $Co_{25}Cr_{25}W_8C_2$ were detected in the deposited layers depending on the powder feeding rate. With further increase in the powder feeding rate, the fractions of W_2C and the bulk (unmelted) WC particles were increased and that of the TiC particle was reduced correspondingly due to the thermal diffusion. The layer thickness increased from 1.3 to 2.7 mm when the powder feeding rate increased from 40 to 100 g min^{-1}, while the dilution ratio decreased from 23 to 5.3% as a result of the thermal diffusion of the laser energy. The microhardness of the composite was found to be three times higher than that recorded for the TC21 substrate (1020 vs. 340 HV$_{0.05}$). The results revealed that the best homogeneous microstructure with the highest microhardness was achieved at the powder feeding rate of 100 g min^{-1} whereas microcracks free layers were accomplished at 40 g min^{-1}.

Keywords TC21 alloy · Direct energy deposition (DED) · Stellite-6 · Tungsten carbide particles (WC) · Microstructure · Layer thickness · Microhardness

1 Introduction

The direct energy deposition (DED) technology includes the use of a laser beam as the heat source to produce a melt pool of powder materials in order to form a deposited layer on a substrate to enhance the surface properties of the materials [1]. TC21 alloy is a recent α + β titanium alloy with the chemical composition of (Ti-6Al-3Mo-2Sn-2Zr-2Nb-1.5Cr-0.1Si), that has been effectively applied to manufacture crucial components, especially in the aerospace industry [2]. This alloy has an outstanding combination of mechanical as well as chemical properties that can be enhanced by controlling its microstructure and workability [3, 4]. Nevertheless, its low hardness, as well as poor tribological performance, restrict the usage of such alloys under severe abrasion conditions which is the main drawback that limits its competitiveness [5]. Therefore, protecting such alloys with hard wear resistance coatings becomes an emerging engineering solution to their poor tribological problems and an effective way to solve this problem. The DED process with metal matrix composites (MMCs) may be used to deposit hard-facing

✉ Samar Reda Al-Sayed
sreda@niles.cu.edu.eg; eng_samar1989@cu.edu.eg

1   Tabbin Institute for Metallurgical Studies (TIMS), Cairo 11731, Helwan, Egypt

2   Department of Engineering Applications of Lasers, National Institute of Laser Enhanced Sciences (NILES) - Cairo University, Giza 12611, Egypt

3   Department of Metallurgy, Faculty of Engineering, Cairo University, Giza 12611, Egypt

coatings on metallic surfaces exposed to abrasive wear. MMCs are composed of hard reinforcing phases that are dispersed in a ductile metal matrix [6]. The reinforcement consists usually of ceramics like titanium, tungsten, or chromium carbides [7, 8]. Different alloys such as Fe-based and Co-based alloys, besides Ni-based alloy, act as the binding phases between the ceramic hard phases and the ductile matrix. Hence, reducing the residual stresses in turn limits the crack formation.

The DED technique of titanium alloys has been studied by numerous researchers, especially in pure titanium [9] and Ti-6Al-4 V alloy [10]. A cladding powder of NiCrBSiC reinforced with hard ceramic WC particles is the most widely applied on the titanium substrate as a high wear-resistant coating. Al-Sayed et al. [11] successfully deposited a blended powder consisting of 60 wt. % tungsten carbide (WC) and 40 wt. % NiCrBSiC on TC4 titanium alloy. A variable laser output power ranging from 600 to 1000 W was used with two corresponding scanning speeds of 25 and 50 cm min^{-1} to attain different laser heat inputs. High-quality clad layers were thus achieved at a laser heat input of 59.5 J mm^{-2}. An enhancement of more than threefold in the microhardness was attained, and the wear resistance was improved by values reaching 400 times. Higher powder feeding rates were also accomplished with various laser interaction times to obtain the optimal conditions for a thicker clad layer with superior mechanical properties [12]. The obtained results indicate that the best clad layer corresponds to a laser interaction time of 0.3 s. A microhardness level was thus increased by more than fourfold.

Some studies have investigated different conventional treatments on TC21 alloy [13–15], whereas scarce studies were reported that considered laser material processing on TC21 alloy, especially the DED process [16]. Texture and microstructure characterization of such alloy were examined after applying laser additive manufacturing (LAM) technique [17], the pre-alloyed TC21 alloy powders were fabricated layer by layer on a forged TC21 plate as the substrate. This study concluded that the formed TC21 alloy is characterized by columnar prior β grains with very fine rib-like α-phase and martensite α'-phase. Other research also investigated different conventional treatments after the laser deposition of TC21 alloy [18]. The shapes and volume fraction of primary α-phase are influenced by the annealing treatment, whereas the shapes and volume fraction of secondary α-phase are mainly affected by the aging treatment.

The data of DED with the preblended powder of Stellite-6 plus WC on TC21 alloy and its effect on microstructure, microhardness, as well as wear resistance have already been published for the first time in our previous work [19]. Three different WC fractions in the Co-based alloy powder were applied to the surfaces of TC21 alloy using a 4 kW continuous-wave fiber-coupled diode laser at a constant powder feeding rate to improve their mechanical properties. The results showed that the optimum composition of the deposited powder is 40% Stellite-6 plus 60% WC.

Presently, no data were reported concerning the effect of DED processing parameters, especially the powder feeding rate on the obtained clad layer characteristics. Consequently, and based on the optimum composition of deposited powder, several powder feeding rates were applied in the present work to estimate the impact of process parameters on quality characteristics and microhardness of the deposited layer. The aim of this work is to attain an appropriate powder feeding rate from the selected processing parameters during the DED process that creates a uniform distribution of hard WC particles which is crack-free and nonporous to enhance the hardness of such alloy. The optimization between processing parameters in DED technology is obviously a high hope of this study.

Additionally, this research work offers a guideline for the range of appropriate powder feeding rates during DED on TC21 substrate as long as the microstructure and the microhardness are concerned.

2 Experimental procedures

2.1 Materials

The present TC21 alloy was received in a cylindrical shape with a diameter of 120 mm and length of 190 mm supplied by Baoji Hanz Material Technology Co., Ltd., Shanxi, China. TC21 samples with $30 \times 30 \times 10$ mm dimensions were cut using a wire cutting machine and utilized as a substrate for the DED process. The determined composition in wt.% is 6.5Al, 2.9Mo 2.2Sn, 2.2Zr, 1.6Cr, 2Nb, 0.1Si, and the balance of Ti. A SEM micrograph of the as-received substrate TC21 alloy is shown in Fig. 1. It exhibits a lamellar microstructure of alpha-phase (α) and beta-phase (β).

Microparticles of 60% WC ceramic powder, 99.9% purity (Technogenia S.A.S, France) with particles ranging in size from 45 to 150 μm preblended with 40% Stellite-6 (Co-based alloy) (Hoganas, Belgium S.A) with a particle size of 40 to 210 μm were used as cladding material. The powder chemical composition in wt.% of WC particles is 4C, 0.23Fe, and balance W and for Stellite-6 is 29.5Cr, 1Mn, 4.8 W, 3Ni, 3Fe, 1.4C, 1.3Si, 1Mo, and balance Co.

2.2 Design of DED experiments

DED experiments were conducted using a 4-kW fiber-coupled diode laser operating at a wavelength of 1050 nm in a continuous-wave mode. DED system consists of 9-axis numerical control working table and an attached coaxial nozzle powder feeder system (TECHNOGENIA Middle

Fig. 1 SEM of as-received TC21 alloy
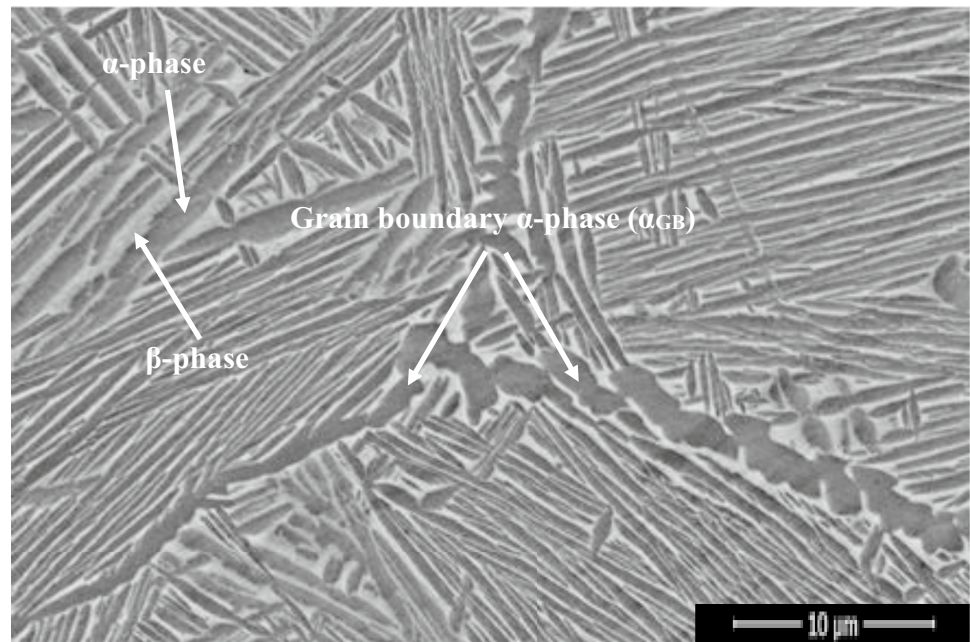
East company, Dubai, UAE). During the DED process, TC21 sample was placed in an area protected by argon gas that was continuously shielded with a flowing rate of 15 L min^{-1} to avoid any oxidation of the melt pool [20, 21]. To investigate the influence of DED process parameters on quality characteristics and microhardness of deposited layer, a series of powder feeding rates were attempted as listed in Table 1. According to our previous work [19], the best mixture composition of deposited powder was 60% WC + 40% Stellite-6. Therefore, the same powder composition was used with different powder feeding rates. For each condition, a deposition zone with an eight-track with 50% overlap was performed in our experiments besides a single track for deposition layer characterization. This range of laser power and scanning speed adopted was intended to only melt the NiCrBSi matrix powder without melting the WC particles and to avoid the high percentage of dilution ratio [11, 12].

Table 1 Laser processing parameters of DED process

Parameters	Value
Laser power	2000 W
Scanning speed	900 mm min^{-1}
Energy density	33.33, 60 J mm^{-2}
Powder feeding rates	20, 40, 60, 80, 100 g min^{-1}
Feeding gas	5 L min^{-1}
Shielding gas	15 L min^{-1}
Defocus distance	16 mm
Beam diameter	3 mm

2.3 Testing of deposited layer characteristics

The quality characteristics of deposited layers were investigated, corresponding to the various powder feeding rates, including the cross-section geometry characterization via the techniques of scanning electron microscope (SEM) with an energy-dispersive X-ray (EDX) microanalyzer (QUANTA FEG 250, FEI, Hillsboro, OR, USA) and X-ray diffractometer (XRD) (XPert Pro Analytical 45 V, 40 mA with source copper 1.54 Å, Poland). This investigation includes the measurement of layer thickness (T), coating width (W), and dilution ratio (D). All samples were ground on SiC grit paper, polished, and etched with a solution of 6 ml nitric acid HNO$_3$ and 2 ml hydrofluoric acid HF (48% concentration) for 1.5 min [12]. Microhardness testing was measured using a Leco LM 7000 micro-hardness tester (Leco Corporation, Connecticut, USA) under a load of 500 g with a time of 15 s.

3 Results and discussion

3.1 Preliminary attempts of DED process at an energy density of 33.33 J mm^{-2}

Deposition laser energy can critically affect the coating quality. In order to investigate the effect of energy density, preliminary attempts (Fig. 2) were made to determine the appropriate energy density value for good deposition quality. Samples were processed at an energy density of 33.33 J mm^2, with a powder feeding rate of 20 and 40 g min^{-1}. At 20 g min^{-1}, the deposited layer exhibits an excellent metallurgical bond with TC21 substrate without any surface cracks.
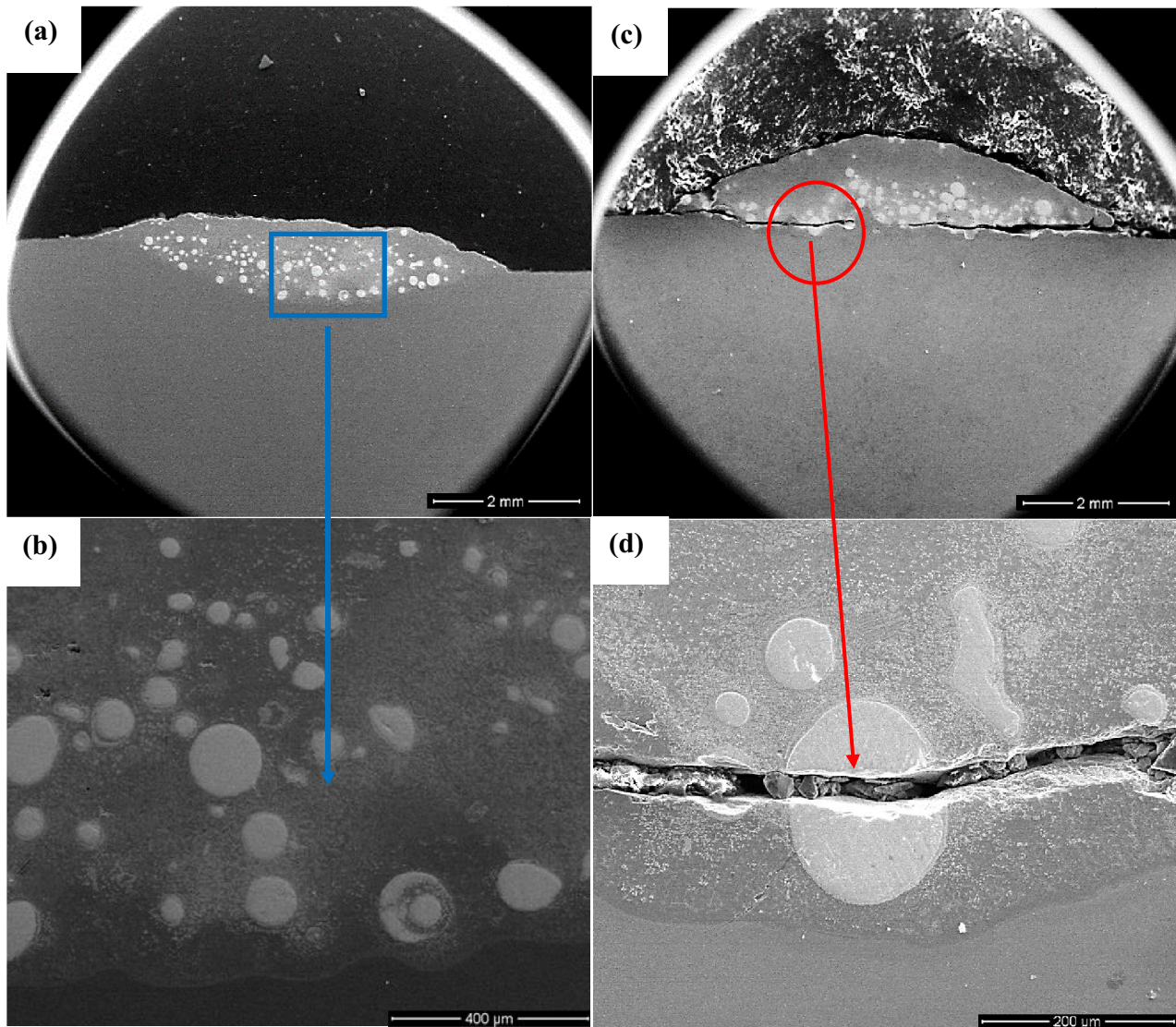
Fig. 2 SEM micrographs of whole deposited area for samples processed at 33.33 J mm^{-2} with feeding rate of **a** 20 g min^{-1}, **b** good metallurgical bond without any surface cracks at 20 g min^{-1}, **c** 40 g min^{-1}, and **d** crack formation through the WC particle at 40 g min^{-1}

While, at 40 g min^{-1}, the microstructure reveals no sufficient bonding between coating and substrate because of the small amount of energy that was delivered to the substrate. Within the low energy density range, the deposition energy is insufficient to completely melt the clad powder, resulting in a rough coating surface. The obtained microstructure shows a heterogeneous dispersion of WC particles in Co alloy solid solution as confirmed from the EDX line scan in Fig. 3. Most WC particles tend to sink into the bottom of the deposition layer, causing interface zone cracks to occur. This is because of the concentration of WC particles that leads to the generation of residual stresses as shown in Fig. 2c. Therefore, the energy density value was doubled, based on our previous studies [11, 12], to ensure the formation of good bonding for all remaining experimental conditions.

3.2 Final attempts of DED process at an energy density of 60 J mm^{-2}

An increase in the energy density to 60 J mm^{-2} was applied for all powder feeding rate values in order to overcome the insufficient metallurgical bonding and cracks in the deposited layer that occurred at the energy density of 33.33 J mm^{-2}. At that level of energy density more powder was melted and the spreading of the molten metals is improved. In order to optimize the powder feeding rate, the deposition energy was fixed at 60 J mm^{-2} to restrain the heat input for the metallurgical reactions between clad powder and titanium substrate. Various powder feeding rates of 40, 60, 80, and 100 g min^{-1} were set to investigate the influence of this parameter.
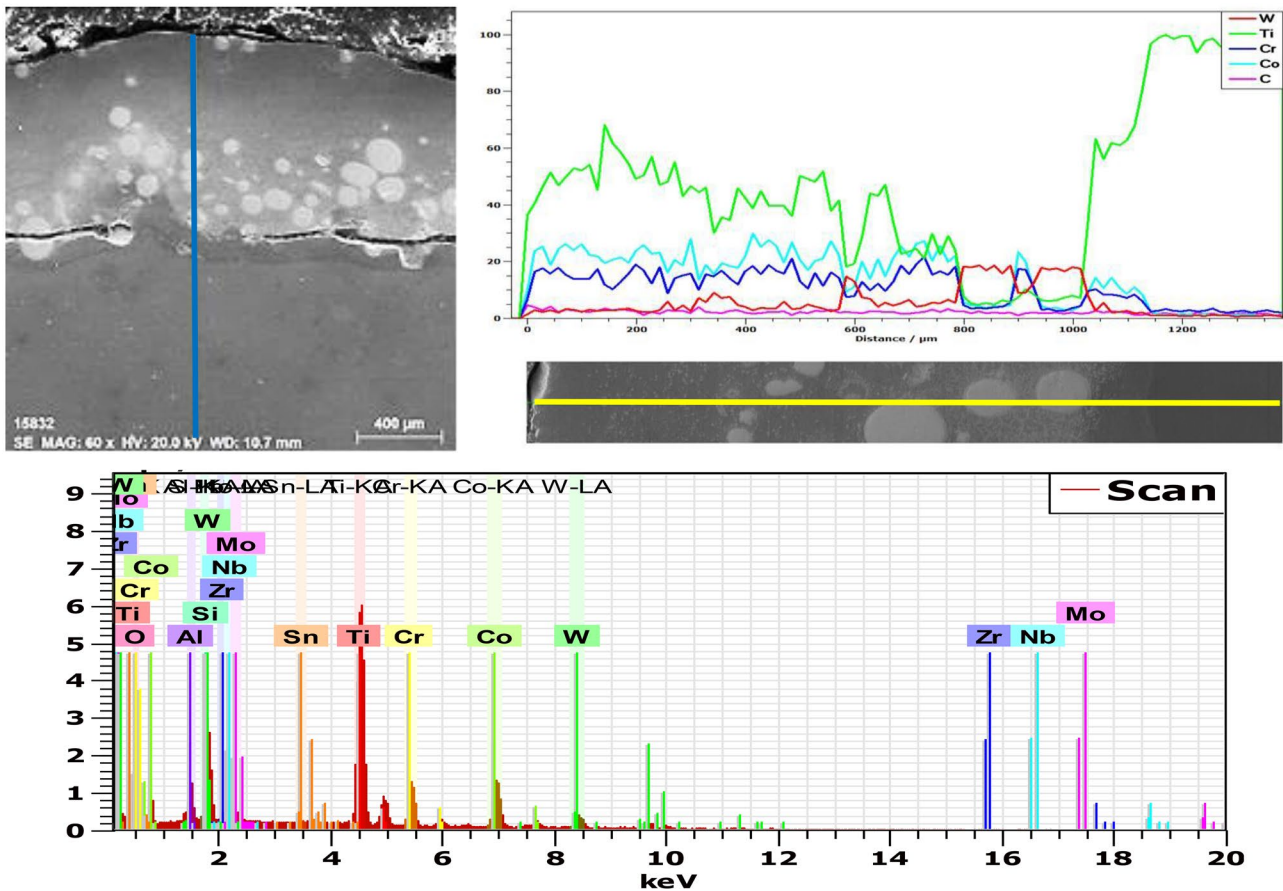
Fig. 3 EDX line scan (40 g min^{-1}) along the cross-section of MMC layer

3.3 Microstructure analysis at an energy density of 60 J mm^{-2}

3.3.1 The Powder feed rate of 40 g min^{-1}

Figure 4 shows the micrographs of samples processed at 40 g min^{-1}. The microstructure consists of three different zones: (a) deposition zone (DZ), (b) interface zone (IZ), and (c) heat-affected zone (HAZ). Almost half of the deposited zone was shown to be free from the bulk WC particles, Fig. 4a. Only Co-based alloy metal matrix coating (MMC) with some clusters was detected at the surface of the coating as presented in Fig. 4b. Accompanying the rise in energy density, the energy absorbed by the molten pool increased and caused a large molten pool from the Co-based alloy and TC21 substrate due to heat diffusion. Consequently, and due to the high density of WC particles, most of them fall into IZ leading to a heterogeneous distribution of WC particles on the coating surface. The IZ contains a fine dendritic structure as shown in Fig. 4c, d. In order to further verify the phase composition and understand the thermal diffusion between the deposition powder and the substrate

alloy, all constituents were analyzed by means of EDX and XRD as illustrated in Figs. 5 and 6, respectively. EDX point analysis confirmed the WC fragmentation in the deposition zone, resulting in the formation of many granular clusters that mainly consisted of W$_2$C and TiC through the MMC. This finding agrees well with the XRD spectral results of clad samples. As less energy density is required for melting less amount of clad powder at the feed rate of 40 g min^{-1}, the thermal interaction between the WC particles and titanium substrate is more intense resulting in the diffusion of titanium substrate and the formation of TiC particles.

3.3.2 The powder feed rate of 60 g min^{-1}

Attempting to avoid heterogeneous distribution of WC particles at the deposited layer surface by applying a powder feeding rate of 40 g min^{-1}, the rate was increased to 60 g min^{-1} as depicted in Fig. 7a. The microstructure showed good metallurgical mixing bond though the bulk WC particles were observed at 580 μm below the top of the deposited layer. The main difference in the MMC microstructure at that powder feeding rate is that the surface coating is much
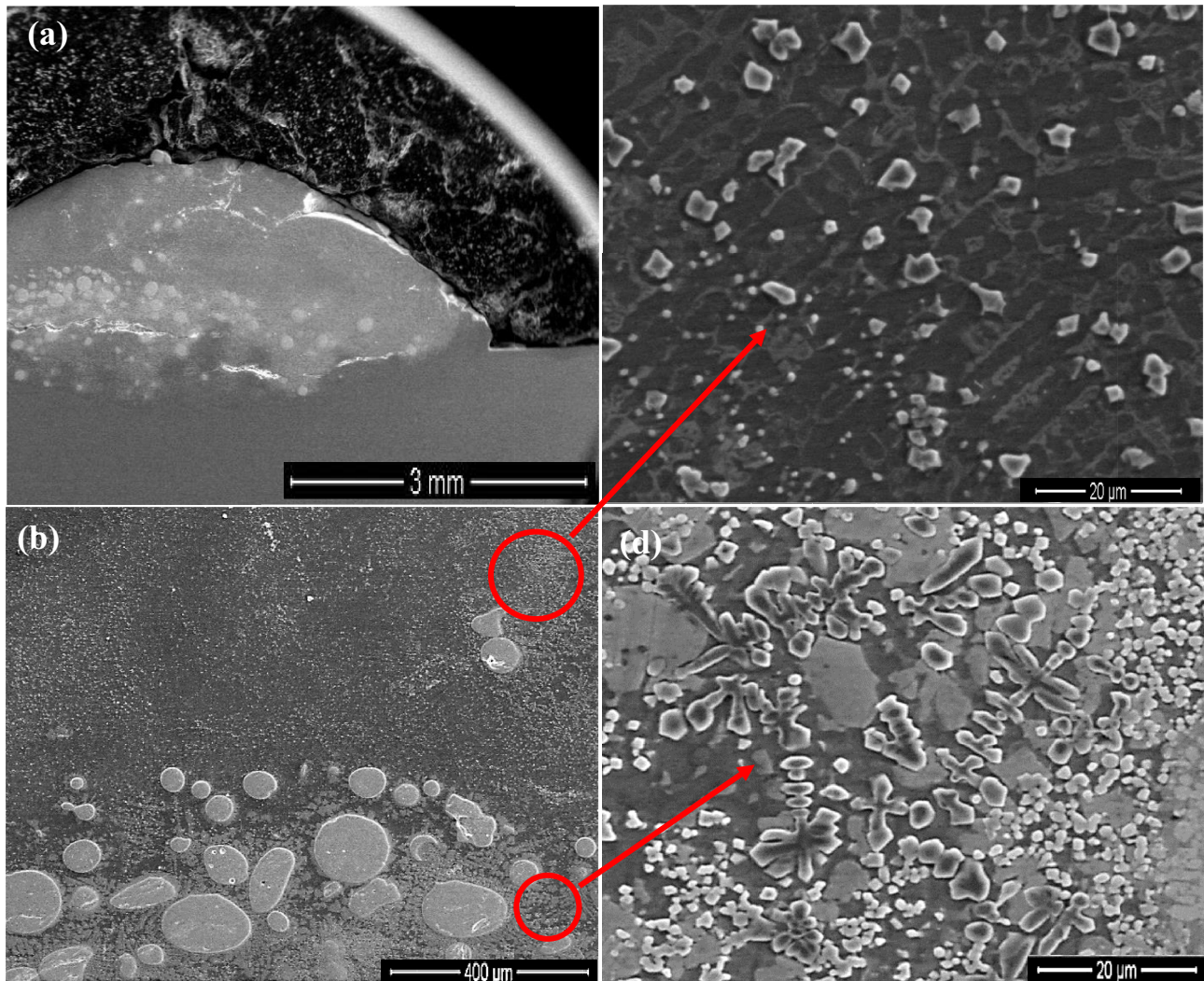
Fig. 4 SEM micrographs of samples processed at 40 g mm^{-1}: **a** whole deposited layer, **b** DZ, **c** higher magnification of the W$_2$C granular clusters, and **d** dendritic structure in IZ

rich in W$_2$C phase and the fragmented W$_2$C in the deposition zone transformed from granular clusters-type to rod-type as presented in Fig. 7b. Additionally, MMC shows a higher WC content with more uniform distribution than that observed in samples processed at a lower rate of 40 g min^{-1}. The IZ contained larger granular clusters of W$_2$C phase, Fig. 7c. The same constituents observed at the powder feeding rate of 40 g min^{-1} were also detected in XRD spectra of the powder feeding rate at 60 g min^{-1}.

The residual stress in composite coating caused small microcracks to form at the interface zone, as seen in Fig. 8. The residual stresses of WC/Co-based (Stellite-6) MMC mainly depend on microstructure-developed stress and induced thermal stresses [22–24]. Owing to ductility as well as the high toughness of Co-based alloy and TC21 substrate, residual stresses may not be capable of causing cracks. However, during rapid heating as well as

cooling of the deposition process, and the different thermal expansion coefficients of WC particles and Stellite-6 Co-based alloy powder, a large temperature differential would generate thermal stresses in WC particles [25].

3.3.3 The powder feed rate of 80 g min^{-1}

The same zones that were observed at 60 g.min^{-1} were also observed at 80 g min^{-1} (Fig. 9). However, the bulk WC particles were detected at 420 μm below the top of the deposited layer, indicating that the increasing powder feed rate increases the local content of the WC and Co-based alloy in the coating surface with a homogeneous distribution of WC particles at the coating surface. The XRD results (Fig. 10) showed that the hypereutectic structure in the deposition zone consisted of the Co-rich γ phase mixed with complex carbides, such as WC, Cr$_7$C$_3$,

Fig. 5 EDX point analysis results of deposited layer processed at 40 g min^{-1}: **a** W$_2$C and **b** TiC


Element	Wt., %
C	8.9
Ti	1.9
Cr	20.6
Co	26.3
W	41.3

Element	Wt., %
C	11.3
Ti	67.5
Cr	5.6
Co	8.6
W	7
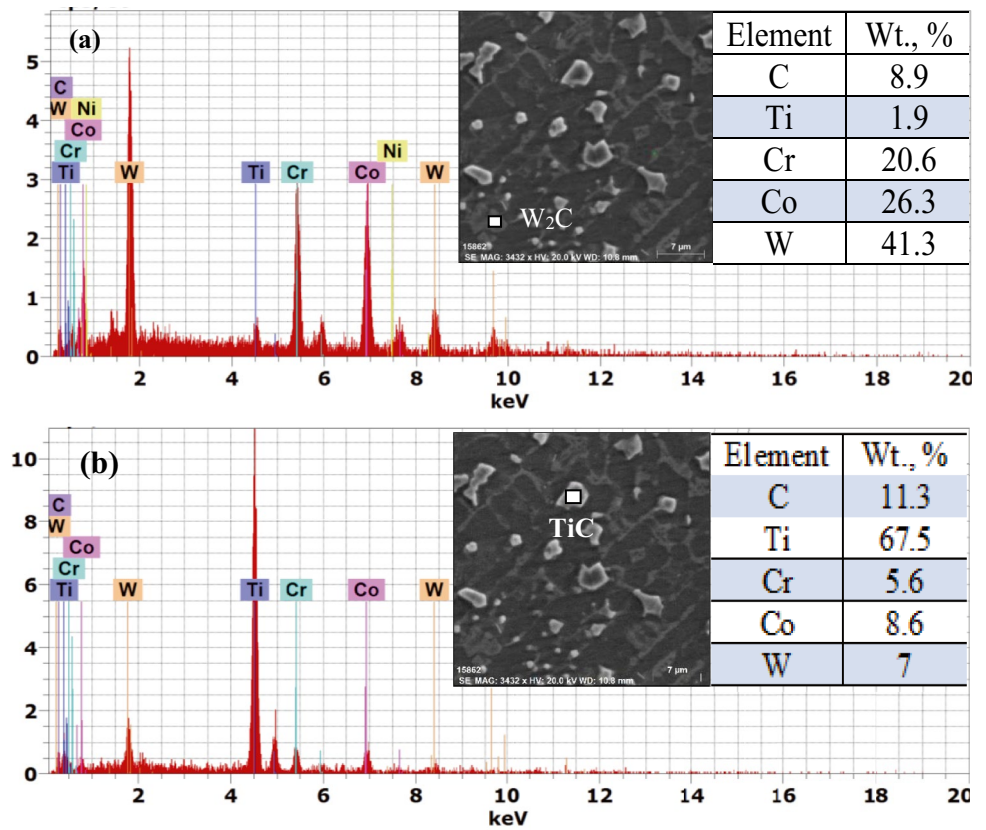
Co$_{25}$Cr$_{25}$W$_8$C$_2$, and W$_2$C. A weak TiC peak can be seen from the XRD pattern. This may be due to the thicker deposition layer which tended to have a lower amount of diffused titanium from the substrate and thus more intermetallic compounds containing carbon, tungsten, and chromium were formed. The appearance of the micro-cracks at the interface zone is attributed to the induced residual stress in the composite coating as discussed before in the case of 60 g min^{-1}.

3.3.4 The powder feed rate of 100 g min^{-1}

With a further increase in feeding rate to 100 g min^{-1}, the deposited layer revealed a dendritic structure with a stable microstructure characteristic of the clad powder. Good bonding of the reinforcement phases by diffusion in the MMC was identified with micro-cracks appearing in the interface zone as seen in Fig. 11a, b, c. Dendrite structures, as well as interdendritic eutectic phases, were found in the matrix,

Fig. 6 X-ray diffraction spectrum of deposition layer with powder feeding rate at 40 g min^{-1}. *Reference codes for each detected phase: 00–027-1125, 00–035-0804, 00–035-0776, 00–003-1172, 01–074-1219, 00–001-1255, respectively

a: Co$_3$W$_3$C
b: Cr$_3$C$_2$
c: W$_2$C
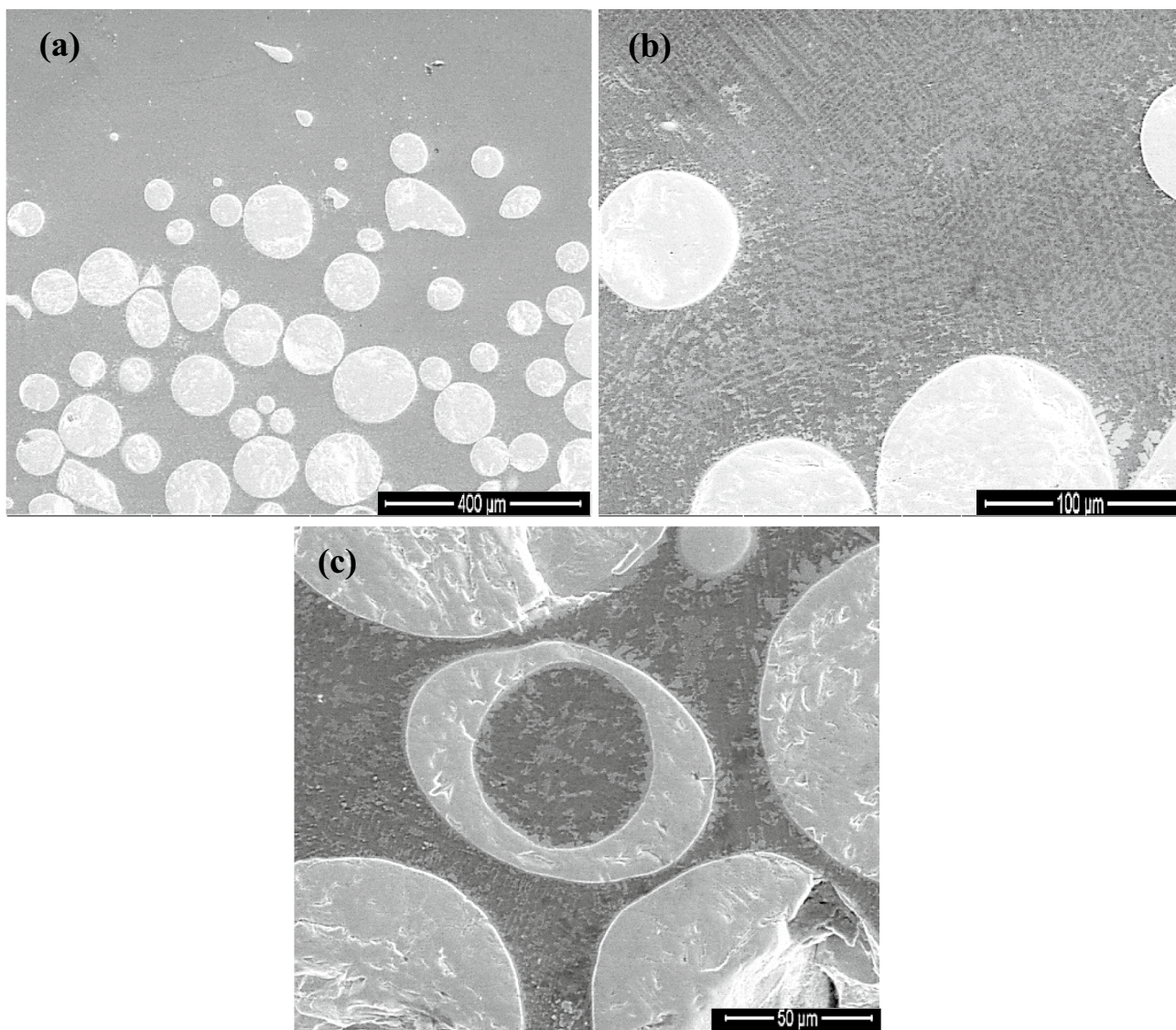d: Cr$_{23}$C$_6$
e: TiC
f: Co
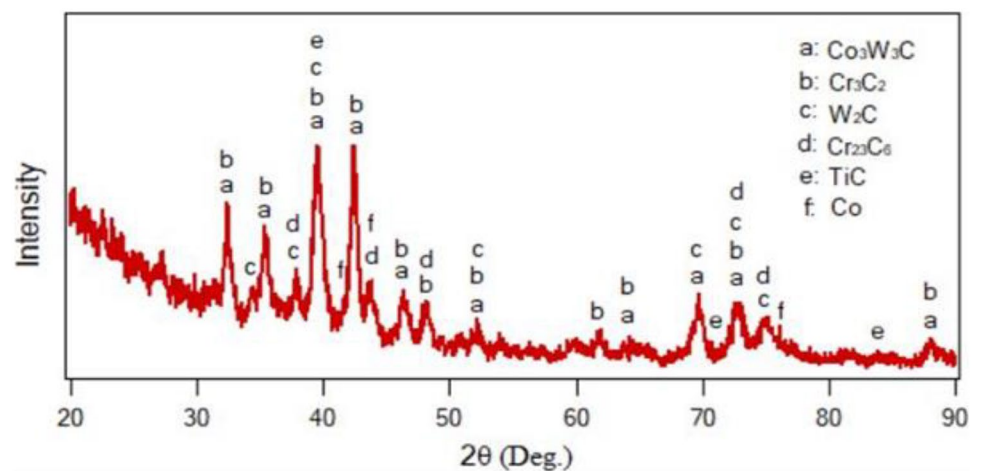
Fig. 7 SEM micrographs of samples processed at 60 g min^{-1}: **a** DZ, **b** IZ with rod-type W$_2$C, and **c** dendritic structure in IZ
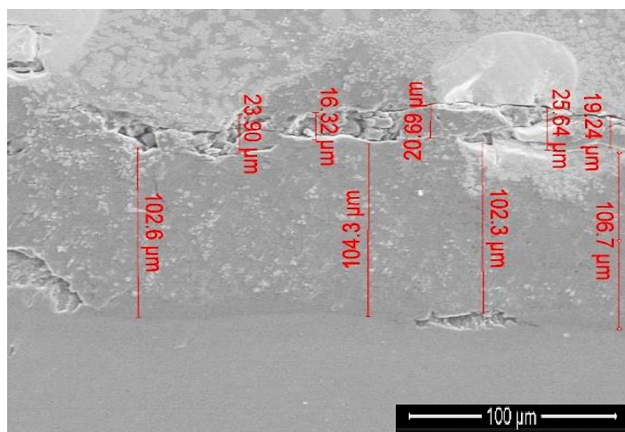

Fig. 8 Micro-crack appeared at IZ for samples processed at powder feeding rate of 60 g min^{-1}

Fig. 11d, e. Larger size and enriched amount of the WC particles were observed due to the higher localized proportion of WC particles in the deposited powder which is beneficial to its hardness. More unmelted WC particles can be found in the upper zone of the deposited layer compared to those processed at lower powder feeding rates. Hence, high thermal stresses were generated in such a brittle structure resulting in the formation of the defected coatings. EDX point analysis observations, Fig. 12, reveal that excessive powder feeding rate during the DED process can cause several metallurgical reactions between WC and Co-based alloy elements. Subsequently, numerous carbides were formed in the melt pool such as tungsten, cobalt, and chromium carbides. In addition, the heat transfer from the substrate alloy is further weakened because more clad powder consumes more laser energy when the powder feeding rate increases
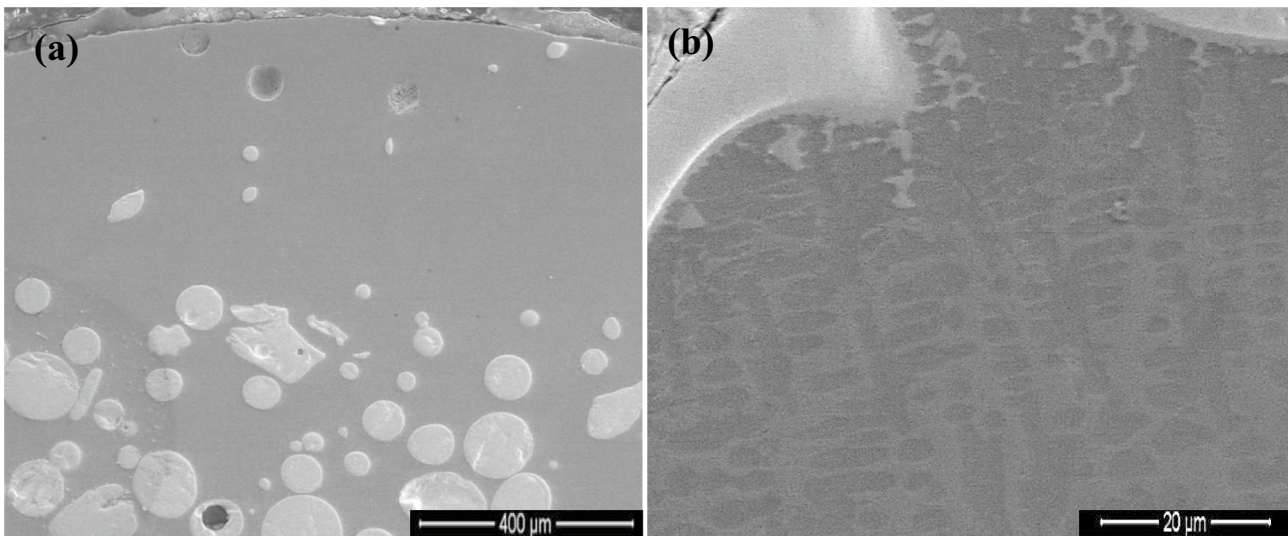
Fig. 9 SEM micrographs of samples processed at 80 g min^{-1}: **a** DZ and **b** dendritic structure in IZ

from 40 to 100 g min^{-1}; thus, TiC particles are not detected as confirmed by small fractions of Ti element in all detected phases.

Crack formation is an extremely complex process and has lots of reasons depending mainly on the residual stresses and mechanical behavior of MMC [26]. As the cooling rates in DED processes are extremely high, liquid to solid transformation during solidification might cause cracking in severe cases. In addition, several solid-state transformations can also induce residual stresses, such as precipitations including volumetric changes [1]. In the present case, the key factor in the induced residual stresses is the precipitation of various complex carbides and brittle intermetallic compounds in MMC, which is reflected from XRD spectra and SEM examination for each powder feed rate condition. If the residual stress

was greater than the material strength, fracture occurred [27]. Clearly, this issue of the residual stresses induced by DED process has to be comprehensively studied and this is hopefully planned in future work. It usually initiates at the interface layer due to the mismatch between the deposition layer and the substrate alloy as observed in our study, see Fig. 13; nevertheless, there is a good mixing bond between the coating layer and substrate. Therefore, it is highly recommended to preheat the substrate to prevent cracking initiation by decreasing the cooling rates and diminishing the induced thermal stress effects [28]. Furthermore, the cracks may easily form due to the big particle size ~ 100 μm for the used powder. Based on the above discussion, it is indicated that the powder flow rate is a critical parameter during the deposition process that highly influence the microstructure characteristics.

Fig. 10 X-ray diffraction spectrum of deposited layer processed at 80 g min^{-1}. *Reference codes for each detected phase: 01–072-0097, 00–035-0776, 00–023-0196, 01–074-1219, 00–036-1482, 00–001-1277, respectively
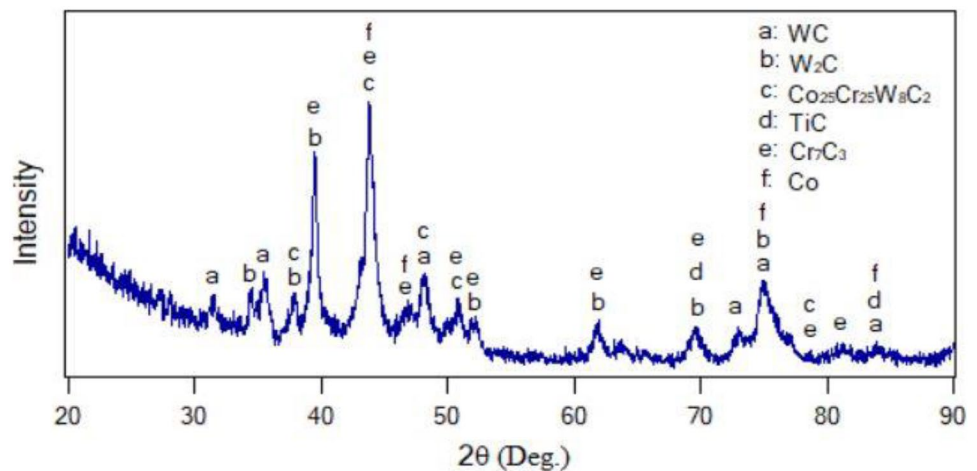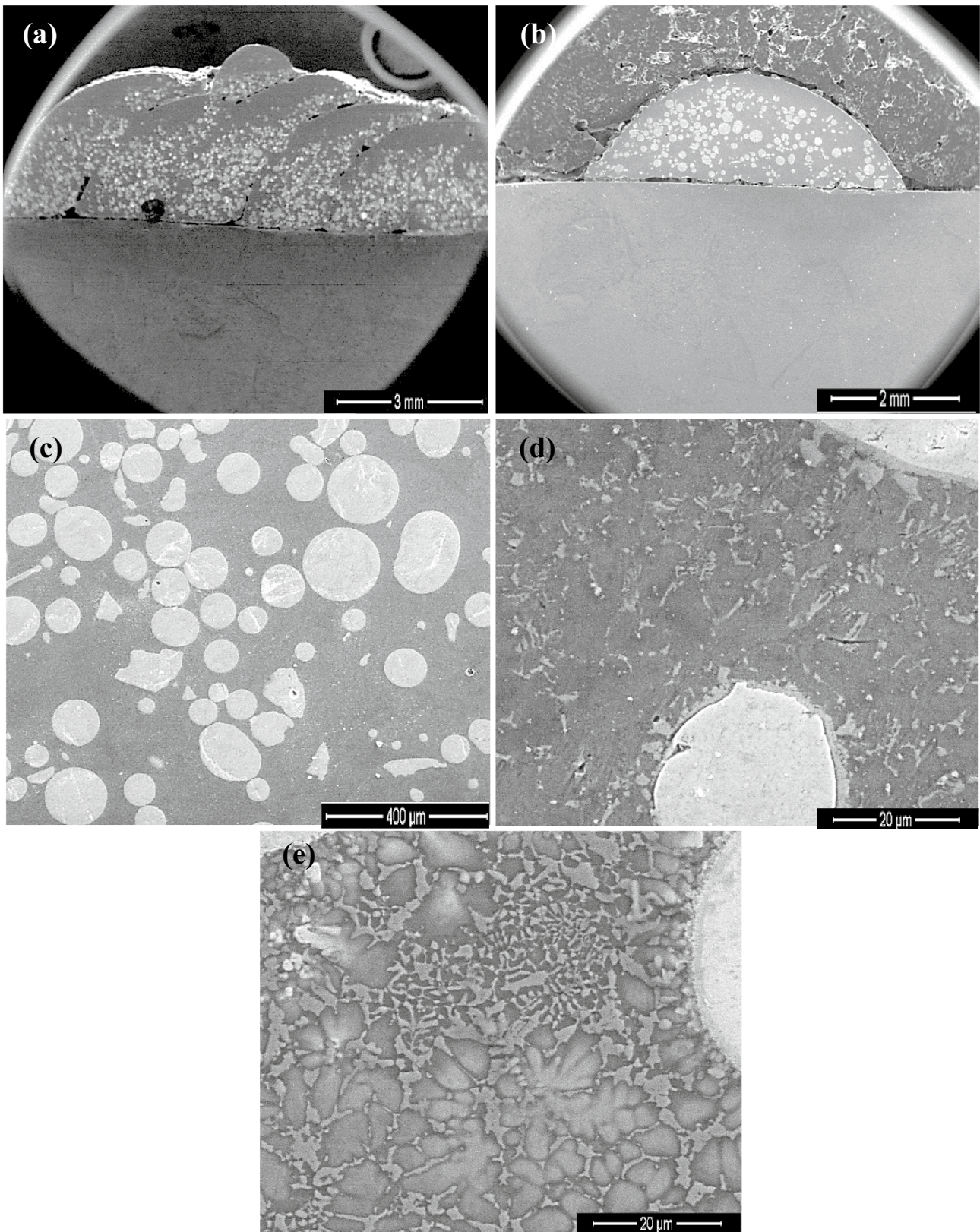
Fig. 11 SEM micrographs at 100 g min^{-1}: **a** multitrack deposited area, **b** cross section of single-track deposited layer, **c** MMC at DZ, and **d** and **e** dendritic structure and interdendritic eutectic phases inside DZ
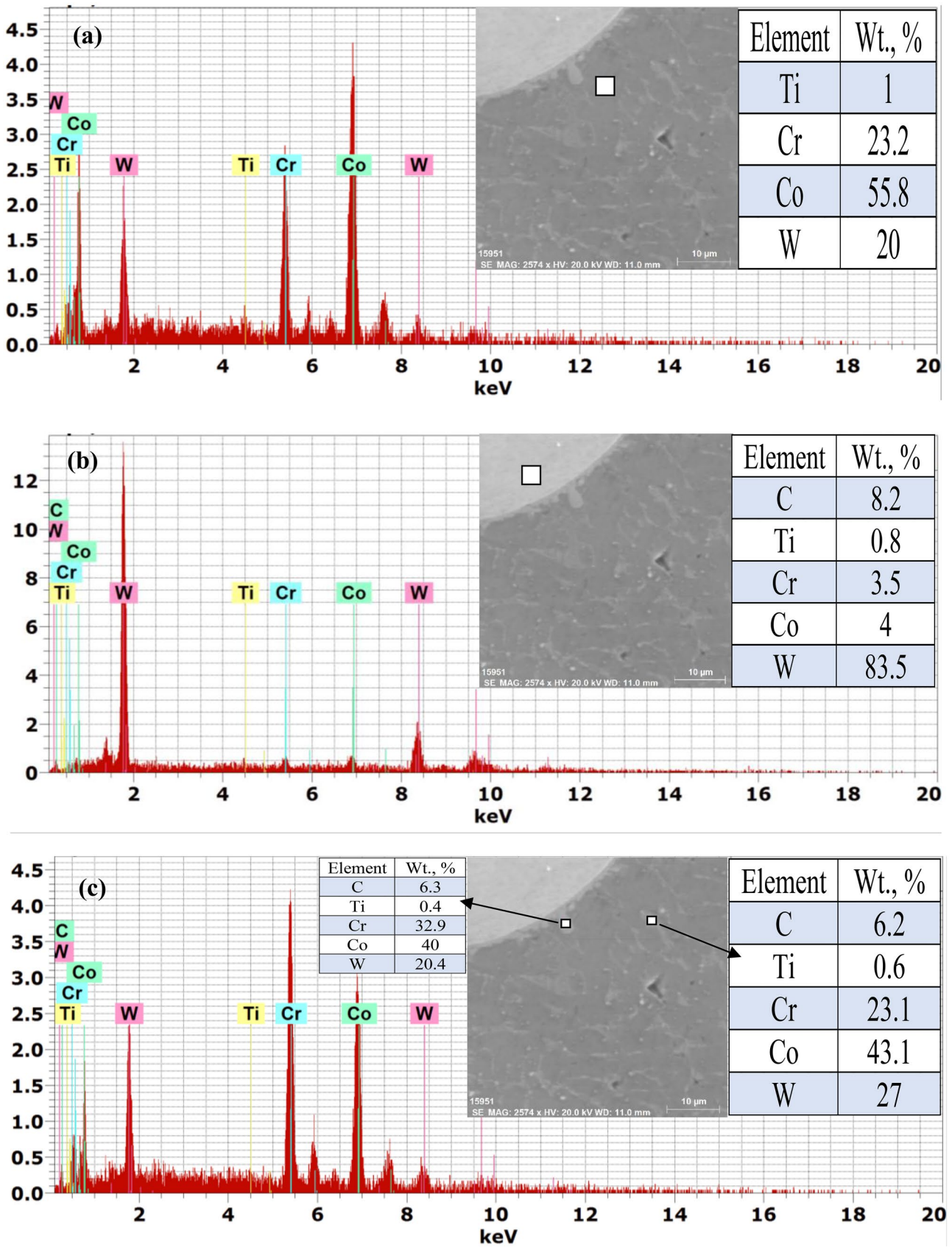
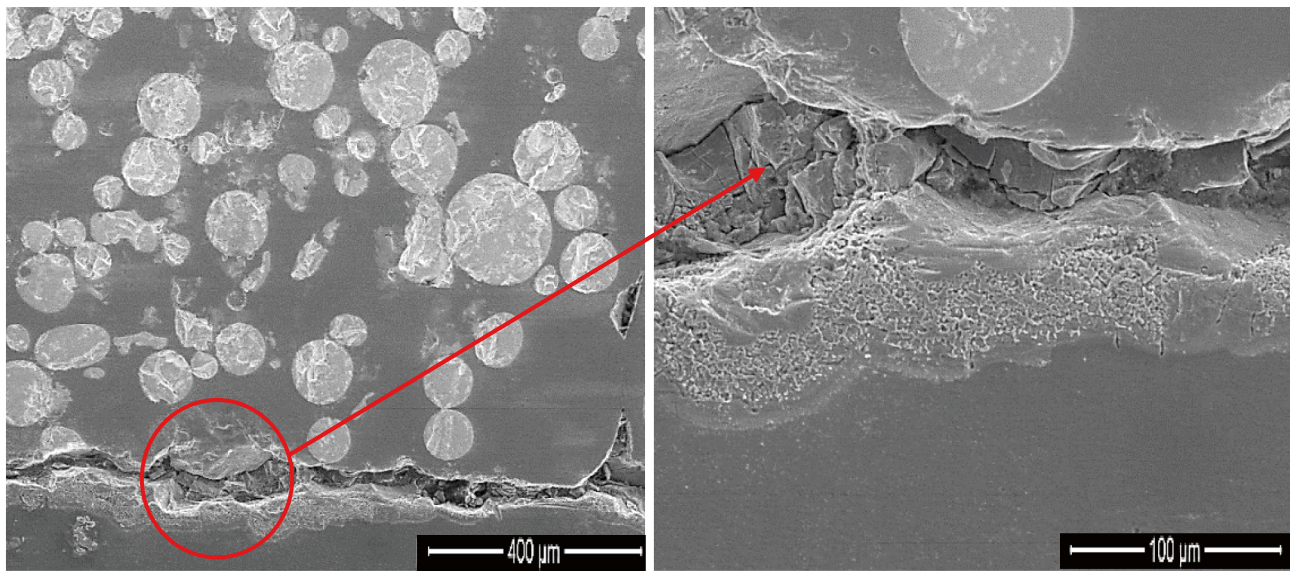**Fig. 12** EDX point analysis results of deposited layer processed at 100 g min⁻¹

Fig. 13 SEM micrographs presenting micro-cracks at IZ for samples processed at 100 g min^{-1}

While the powder feeding rate was raised from 40 to 100 g min^{-1}, more powder was melted and more laser energy was absorbed; therefore, less energy density contributes to the metallurgical reactions among the powder elements and the titanium substrate. The microstructure of the deposited layer was found to be susceptible to the thermal effect of laser energy density. With the lowest powder feeding rate of 40 g min^{-1}, the deposited layer contains numerous TiC particles due to the strong thermal effect of laser energy. When increasing the powder feeding rate to 100 g min^{-1}, the deposited layer mainly composed of intermetallic compounds and complex carbides and more amount of unmelted WC particles. This means that with further increase in the powder feeding rate the fraction of W$_2$C phase and the fraction of bulk (unmelted) WC particles were both increased and that of TiC particle was reduced correspondingly. Accordingly, as the formation of hard intermetallic compounds and tungsten carbides is restrained at a higher powder feeding rate, it will be reflected on the results of the microhardness.

On the other side, one cannot ignore the good advances of DED on the obtained microstructure because of the new relations between grain structures and grain growth with respect to anisotropy [29]. In DED process, the grain structure and laser power are closely related, in which the energy density value can be the key in any additive manufacturing method to control the grain structure [30]. In future work, it is planned to investigate the effect of different energy densities on the grain structure concerning anisotropy.

3.4 Deposition layer characteristics

The effects of varying the powder feeding rate at an energy density of 60 J mm^{-2} and four different powder feeding rates on the deposited layer characteristics was traced via SEM under the same magnification as shown in Fig. 14. Apparently, the thickness of the coating linearly increased from 1.3 to 2.7 mm with an increase in powder feeding rate from 40 to 100 g min^{-1}. Meanwhile, the deposited layer width (W) slightly decreased from 6.2 to 4.97 mm. The powder flow rate is thus a significant parameter of the DED process that significantly affects the deposited layer thickness.

Another important quality characteristic of the deposited layer is the dilution ratio (D) [2, 7]. This is the mixing of substrate alloy with clad material. A minimum dilution is necessary to guarantee a good metallurgical bond between the cladding and substrate, whereas an excessive dilution is unfavorable. A preservation of the chemical composition and properties of the coating is required. The dilution ratio of the deposited layers was calculated based on the clad layer geometry by the following equation according to some authors [11, 31]:

$$D = H_2/(H_1 + H_2) \tag{1}$$

where H$_2$ is the melt depth in the substrate and H$_1$ is the clad height.

Accordingly, the dilution ratio decreases from 25 to only 5.3% as the powder feeding rate increases from 40 to 100 g min^{-1}. As the thermal interaction between the
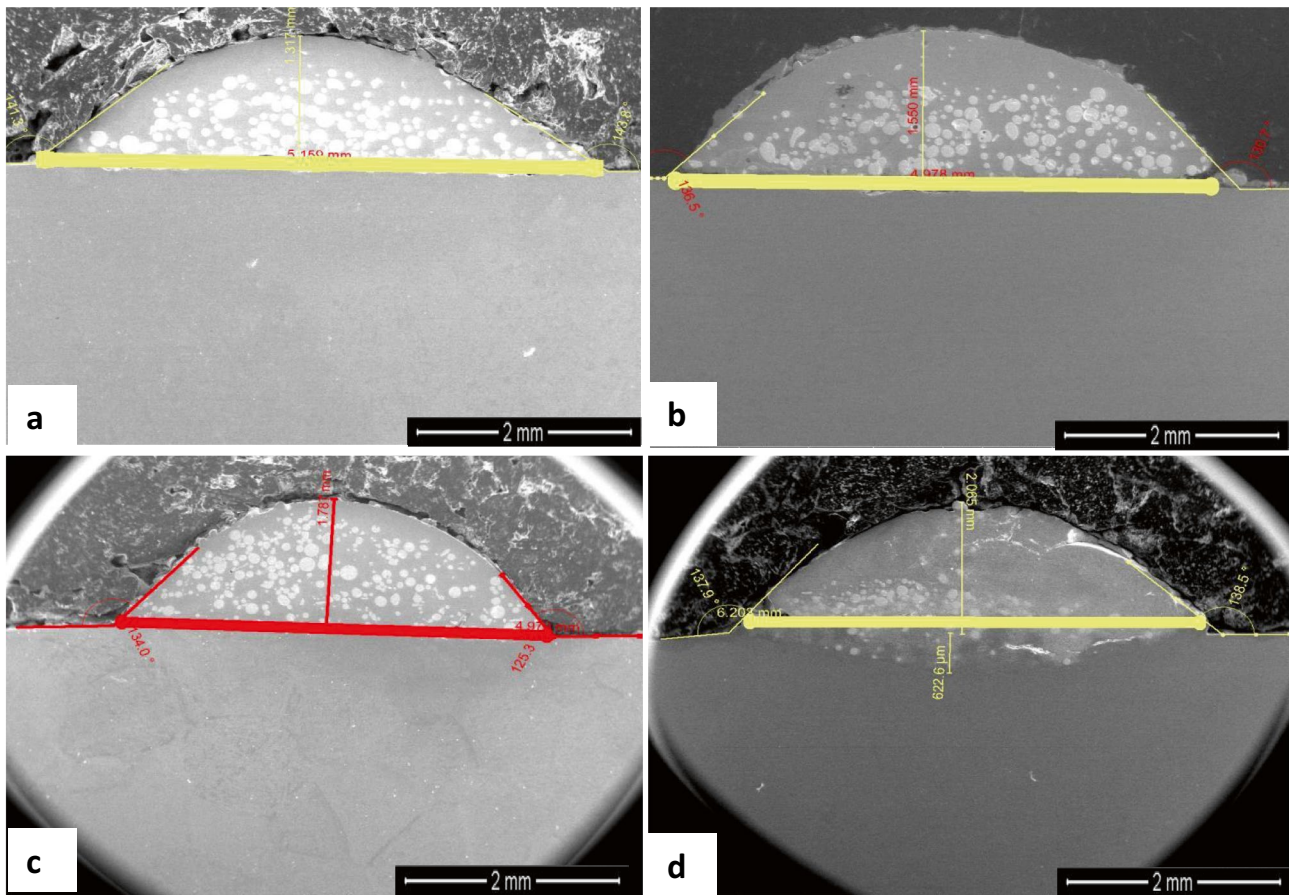
Fig. 14 Deposited layer thickness at different feeding rates: (**a**) 40, (**b**) 60, (**c**) 80, and 100 g min^{-1}

clad powder and titanium substrate is stronger in case of low powder feeding rate compared to other thick coatings, the thin powder layer was overmuch diluted by the metal molten substrate. Table 2 summarizes the data collected after the DED process (60 J mm^{-2}) of single bead for powder feeding rates of 40, 60, 80, and 100 g min^{-1}.

3.5 Microhardness distribution

Microhardness measurements were carried out over the whole deposited layer and along the depth as well. Due to the improvement of the microstructure after the DED process, all deposited layers exhibit high hardness levels above 900 HV$_{0.05}$.

Table 2 Data collected from the DED process (60 J mm^{-2}) at different feeding rates

Condition	Thickness (T), mm	Width (W), mm	Dilution ratio, %
40 g min^{-1}	1.3	6.2	23
60 g min^{-1}	1.55	5.16	14
80 g min^{-1}	1.78	4.97	9
100 g min^{-1}	2.7	4.97	5.3

The microhardness of MMC is about three times higher than that of TC21 substrate of 340 HV$_{0.05}$. Based on the structure with a high unmelted amount of WC particles at the highest powder feeding rate, the microhardness of MMC increases from 960 to 1020 HV$_{0.05}$ with an increase in powder feeding rate. This range of microhardness values is due to the degradation of the WC particles distribution that is embedded in the Co-matrix with the increase in powder feeding rate. The microhardness is also affected by the fraction of the secondary carbides formed by solid-state precipitation such as W$_2$C, TiC, Cr$_7$C$_3$, Cr$_{23}$C$_7$, and W$_8$C$_2$ during the DED process, and the brittle intermetallic compounds like Co$_{25}$Cr$_{25}$ and Co$_3$W$_3$C since such crystalized phases play a major role in increasing hardness values. This is in accord with previous work [32]. As the excessive hard intermetallic compounds benefit the hardness of the titanium substrate, it is also found that high residual stresses were generated as a result of such hard phases.

The MMC structure surrounding fragmented W$_2$C particles shows microhardness levels decreasing with rising powder feeding rate as presented in Fig. 15. This could be due to a decrease in energy density being applied to the deposited powder with a higher powder feeding rate. This may tend to preserve the high

Fig. 15 Microhardness of MMC surrounding the W_2C clusters versus the powder feeding rates
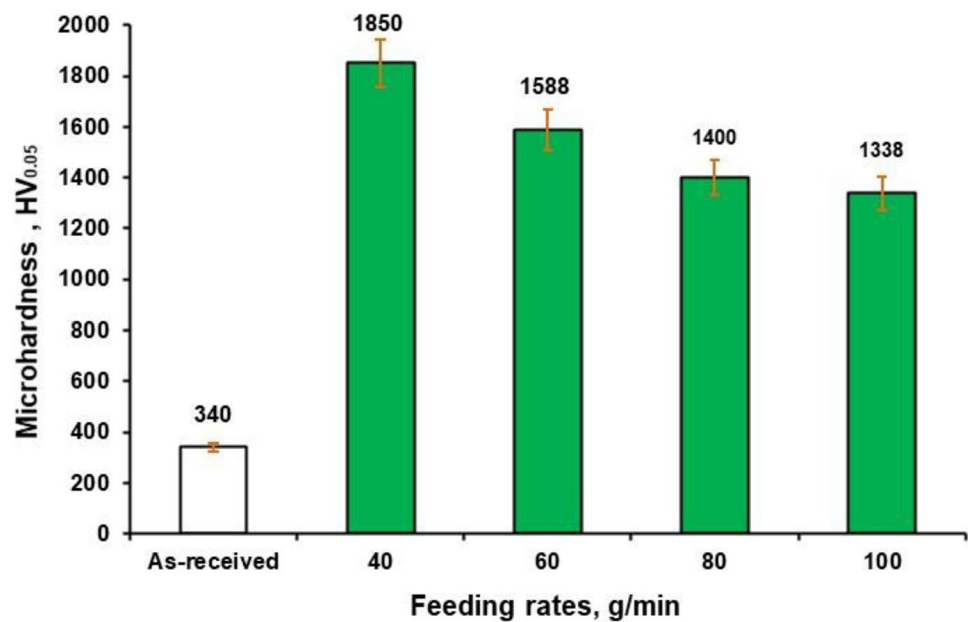
hardness WC particles without fragmentation into W_2C clusters. In addition, the slow cooling rate accompanying with high powder feeding rate leads to the decrease in the dissolution of the carbon in the matrix which results in decreasing the hardness levels. Meanwhile, microhardness of the interface zone as well as the heat-affected zone remained almost in the same range for all different powder feeding rates (~ 680 and ~ 460 $HV_{0.05}$), respectively. The sudden decrease in the microhardness in the interface zone is due to the dilution from the TC21 titanium substrate.

To summarize, the hardness reflects strong dependence on the microstructure of the deposited layer which is highly influenced by the powder feeding rate. However, increasing the deposition layer thickness is a proper way to enhance the hardness property, it is necessary to consider the microstructure and cracks that occurred due to the laser processing parameters.

3.6 Future work

1. A comprehensive study of the residual stresses induced in the microstructure of direct energy deposited samples based on different DED parameters.
2. Replacement of the feeding powder with a feeding wire to solve the problem of the heterogeneous distribution of WC particles in the deposited layer at higher powder feeding rates.

4 Conclusions

The present work deals with the application of DED process to TC21 alloy with different powder feeding rates. The main outcomes are outlined below:

- At specific heat of 33.33 J mm^{-2} and powder feeding rate of 40 g min^{-1}, insufficient bonding between the deposited layer and TC21 substrate was detected with heterogeneous distribution of WC particles in the deposited layer. Most WC particles existed and concentrated in the bottom region of the deposited layer causing cracks in the interface zone.
- Elevation of specific heat from 33.33 to 60 J mm^{-2} at all powder feeding rates tends to yield a good metallurgical bond, though, there was a nonuniform distribution of WC particles in the deposited layer at lower powder feeding rates especially, at 40 and 60 g min^{-1}.
- Several complex carbides and intermetallic compounds such as W_2C, TiC, Cr_7C_3, Co_3W_3C, and $Co_{25}Cr_{25}W_8C_2$ were precipitated in deposited layers and strongly depend on the powder feeding rate. As the powder feeding rate increases the fraction of W_2C particle as well as that of bulk (unmelted) WC particles were increased and that of TiC particle was reduced correspondingly due to the influences of thermal diffusion of the laser energy.
- Layer thickness increased from 1.3 to 2.7 mm with the increase in the powder feeding rate from 40 to 100 g min^{-1}. Whereas the dilution ratio decreased from 23 to 5.3%. This is the fact due to that the thermal interaction between the deposited powder and titanium substrate is stronger in the case of a low powder feeding rate.
- The microhardness of MMC was found to be three-fold higher (1020 $HV_{0.05}$) than that recorded of TC21 substrate (340 $HV_{0.05}$) at the highest powder feeding rate. This may be attributed to the enhancement of the microstructure homogeneity with further increase of the hard intermetallic compounds and complex carbides as identified by XRD analysis.

- The hard intermetallic compounds are beneficial for the hardness property of the titanium substrate, however high residual stresses were generated as a result of such hard phases causing undesirable microcracks in the interface zone.
- The present results reveal that more homogeneous microstructures with the highest possible microhardness were achieved at the powder feeding rate of 100 g min^{-1} whereas the best quality layers free of microcracks were accomplished at 40 g min^{-1}.

Author contribution Conceptualization, R.N.E., A.M.E., A.A.H., and S.R.A.-S.; methodology, R.N.E., A.M.E. and S.R.A.-S.; validation, A.M.E., A.A.H., R.N.E., and S.R.A.-S.; formal analysis, A.M.E. R.N.E., and S.R.A.-S.; investigation, R.N.E., A.M.E., and S.R.A.-S.; resources, R.N.E.; data curation, A.M.E., R.N.E., and S.R.A.-S.; writing—original draft preparation, A.M.E., and S.R.A.-S.; writing—review and editing, R.N.E., S.R.A.-S., and A.A.H.; visualization, R.N.E., A.M.E., and S.R.A.-S.; supervision, R.N.E., A.A.H., and S.R.A.-S. All authors have read and agreed to the published version of the manuscript.

Data availability All data generated or analyzed during this study are included in this published article (and its supplementary information files).

Code availability Not applicable.

Declarations

Ethics approval Not applicable.

Consent for publication All authors have read and agreed to the published version of the manuscript.

Conflict of interest The authors declare no competing interests.

References

1. Dutta B (2020) Directed energy deposition (DED) technology. Encycl Mater Met Alloys 66–84. https://doi.org/10.1016/b978-0-12-819726-4.00035-1
2. Guo X, Zhang J, Chen B, Li J (2020) Effects of triple heat treatment on microstructure and the dry sliding wear of TC21 titanium alloy. IOP Conf Ser Mater Sci Eng 768:2–8. https://doi.org/10.1088/1757-899X/768/2/022067
3. Elshaer RN, Ibrahim KM (2020) Effect of cold deformation and heat treatment on microstructure and mechanical properties of TC21 Ti alloy. Trans Nonferrous Met Soc China English Ed 30:1290–1299. https://doi.org/10.1016/S1003-6326(20)65296-7
4. Elshaer RN, Ibrahim KM, Ahmed MA, Ahmed I (2020) Effect of cooling rate and aging process on wear behavior of TC21 Ti-alloy. Key Eng Mater 835 KEM:265–273. https://doi.org/10.4028/www.scientific.net/KEM.835.265
5. Al-Sayed SR, Abdelfatah A (2020) Corrosion behavior of a laser surface-treated alpha–beta 6/4 titanium alloy. Metallogr Microstruct Anal 9:553–560. https://doi.org/10.1007/s13632-020-00667-w
6. Ibrahim KM, El-Hakeem AMM, Elshaer RN (2013) Microstructure and mechanical properties of cast and heat treated Ti-6.55Al-3.41Mo-1.77Zr alloy. Trans Nonferrous Met Soc China (English Ed 23:3517–3524. https://doi.org/10.1016/S1003-6326(13)62896-4
7. Youssef D, Al-Sayed SR (2021) Microscale clad thickness measurement after laser cladding via laser speckle photography. In: NILES 2021 - 3rd Novel Intelligent and Leading Emerging Sciences Conference, Proceedings. Institute of Electrical and Electronics Engineers Inc., pp 413–415
8. Al-Sayed SR, Youssef D (2021) Exploiting local contrast laser speckle photography for surface topometry of laser metal deposition. In: Laser Congress 2021 (ASSL,LAC). Optica Publishing Group, 2021, Washington, DC United States, p paper JM3A.60
9. Bajda S, Liu Y, Tosi R et al (2021) Laser cladding of bioactive glass coating on pure titanium substrate with highly refined grain structure. J Mech Behav Biomed Mater 119:104519. https://doi.org/10.1016/j.jmbbm.2021.104519
10. Hussein AA, Al-Sayed SR, Elnaby SIH et al (2018) Prominent achievements of laser surface treatment of martensitic stainless steel and alpha-beta 6/4 titanium alloy. Key Eng Mater 786:87–97. https://doi.org/10.4028/www.scientific.net/KEM.786.87
11. Al-Sayed Ali S, Hussein A, Nofal A et al (2017) Laser powder cladding of Ti-6Al-4V α/β alloy. Materials (Basel) 10:1178. https://doi.org/10.3390/ma10101178
12. Al-Sayed Ali SR, Hussein AHA, Nofal A et al (2019) A contribution to laser cladding of Ti-6Al-4V titanium alloy. Metall Res Technol 116. https://doi.org/10.1051/metal/2019060
13. Elshaer RN (2022) Effect of initial α-phase morphology on microstructure, mechanical properties, and work-hardening instability during heat treatment of TC21 Ti-alloy. Metallogr Microstruct Anal. https://doi.org/10.1007/s13632-022-00840-3
14. Elshaer RN, Abdelhameed M, Ibrahim KM et al (2022) Static and fatigue characteristics of heat-treated Ti–6Al–3Mo–2Zr–2Sn–2Nb–1.5Cr–0.1Si alloy. Metallogr Microstruct Anal. https://doi.org/10.1007/s13632-022-00856-9
15. Elshaer RN, El-Deeb MSS, Mohamed SS, Ibrahim KM (2022) Effect of strain hardening and aging processes on microstructure evolution, tensile and fatigue properties of cast Ti-6Al-2Sn-2Zr–2Mo-1.5Cr-2Nb-0.1Si alloy. Int J Met 16:723–737. https://doi.org/10.1007/s40962-021-00622-7
16. Zhang Q, Chen J, Wang L et al (2016) Solidification microstructure of laser additive manufactured Ti-6Al-2Zr-2Sn-3Mo-1.5Cr-2Nb titanium alloy. J Mater Sci Technol 32:381–386. https://doi.org/10.1016/j.jmst.2015.11.019

17. Zhang Q, Chen J, Guo P et al (2015) Texture and microstructure characterization in laser additive manufactured Ti-6Al-2Zr-2Sn-3Mo-1.5Cr-2Nb titanium alloy. Mater Des 88:550–557. https://doi.org/10.1016/j.matdes.2015.09.053

18. Zhuo L, Changmeng L, Dong L, Huaming W (2014) Effect of heat treatment on microstructure and tensile properties of laser deposited titanium alloy TC21. Mater Res Innov 18:S4929–S4932. https://doi.org/10.1179/1432891714Z.000000000812

19. Elshazli AM, Elshaer RN, Hamid A et al (2021) Laser surface modification of TC21 (α / β) titanium alloy using a direct energy deposition (DED) process. Micromachines 12:739

20. Al-Sayed SR, Elshazli AM, Hussein AHA (2020) Laser surface hardening of Ni-hard white cast iron. Metals (Basel) 10:1–19. https://doi.org/10.3390/met10060795

21. Al-Sayed SR, Hussein AA, Nofal AA et al (2017) Characterization of a laser surface-treated martensitic stainless steel. Materials (Basel) 10:595. https://doi.org/10.3390/ma10060595

22. Lee C, Park H, Yoo J et al (2015) Residual stress and crack initiation in laser clad composite layer with Co-based alloy and WC + NiCr. Appl Surf Sci 345:286–294. https://doi.org/10.1016/j.apsusc.2015.03.168

23. Liu J, Jiang H, Lei Z et al (2022) Analysis of the residual stress in additive manufacturing of Ti-6Al-4V. J Phys Conf Ser 2206.https://doi.org/10.1088/1742-6596/2206/1/012011

24. Sun X, Zhao Y, Yang W et al (2022) Novel strategy for reducing residual stress in titanium alloy parts obtained via additive manufacturing. Met Mater Int 2022:1–11. https://doi.org/10.1007/S12540-022-01179-8

25. Youssef D, Hassab-Elnaby S, Al-Sayed SR (2022) New 3D model for accurate prediction of thermal and microstructure evolution of laser powder cladding of Ti6Al4V alloy. Alexandria Eng J 61:4137–4158. https://doi.org/10.1016/j.aej.2021.09.014

26. Xiaodong Z, Shiyun D, Binshi XU, Qingfen LI Control measures for clad cracks of laser cladding remanufacturing. Optimization 1

27. Wen X, Wan M, Huang C, Lei M (2019) Strength and fracture toughness of TC21 alloy with multi-level lamellar microstructure. Mater Sci Eng A 740–741:121–129. https://doi.org/10.1016/j.msea.2018.10.056

28. Wang J, Li L, Tao W (2016) Crack initiation and propagation behavior of WC particles reinforced Fe-based metal matrix composite produced by laser melting deposition. Opt Laser Technol 82:170–182. https://doi.org/10.1016/j.optlastec.2016.03.008

29. Pérez-Ruiz JD, Marin F, Martínez S et al (2022) Stiffening near-net-shape functional parts of Inconel 718 LPBF considering material anisotropy and subsequent machining issues. Mech Syst Signal Process 168:1–18. https://doi.org/10.1016/j.ymssp.2021.108675

30. Pérez-Ruiz JD, de Lacalle LNL, Urbikain G et al (2021) On the relationship between cutting forces and anisotropy features in the milling of LPBF Inconel 718 for near net shape parts. Int J Mach Tools Manuf 170. https://doi.org/10.1016/j.ijmachtools.2021.103801

31. Hemmati I, Ocelík V, De Hosson JTM (2012) Dilution effects in laser cladding of Ni-Cr-B-Si-C hardfacing alloys. Mater Lett 84:69–72. https://doi.org/10.1016/j.matlet.2012.06.054

32. Al-Sayed SR, Elgazzar H, Nofal A (2022) Microstructure evaluation and high-temperature wear performance of hard protective layer deposited on titanium alloy via laser metal deposition. Met Mater Int 2022:1–14. https://doi.org/10.1007/S12540-021-01160-X